Modulation of Stemness and Differentiation Regulators by Valproic Acid in Medulloblastoma

Natália Hogetop Freire [1,2,3] • Alice Laschuk Herlinger [2,3] • Julia Vanini [2,3] • Matheus Dalmolin [3,4,5] • Marcelo A. C. Fernandes [3,4,5,6] • Carolina Nör [7,8] • Vijay Ramaswamy [7,8,9,10] • Caroline Brunetto de Farias [1,2,3] • André Tesainer Brunetto [1,2,3] • Algemir Lunardi Brunetto [1,2,3] • Lauro José Gregianin [2,3,11,12] • Mariane da Cunha Jaeger [1,2,3] • Michael D. Taylor [7,8,10,13,14,15,16,17,18,19,20] • Rafael Roesler [2,3,21]

1 Children's Cancer Institute (ICI), Porto Alegre, RS, Brazil.

2 Cancer and Neurobiology Laboratory, Experimental Research Center, Clinical Hospital (CPE-HCPA), Federal University of Rio Grande do Sul, Porto Alegre, RS, Brazil

3 National Science and Technology Institute for Children's Cancer Biology and Pediatric Oncology-INCT BioOncoPed, Porto Alegre, RS, Brazil

4 InovAI Lab, nPITI/IMD, Federal University of Rio Grande do Norte, Natal, RN, Brazil

5 Bioinformatics Multidisciplinary Environment (BioME), Federal University of Rio Grande do Norte, Natal, RN, Brazil

6 Department of Computer Engineering and Automation, Federal University of Rio Grande do Norte, Natal, RN, Brazil

7 The Arthur and Sonia Labatt Brain Tumour Research Centre, The Hospital for Sick Children, Toronto, ON, Canada

8 Developmental and Stem Cell Biology Program, The Hospital for Sick Children, Toronto, ON, Canada

9 Division of Haematology/Oncology, The Hospital for Sick Children, Toronto, ON, Canada

10 Department of Medical Biophysics, University of Toronto, Toronto, ON, Canada

11 Department of Pediatrics, School of Medicine, Federal University of Rio Grande do Sul, Porto Alegre, RS, Brazil

12 Pediatric Oncology Service, Clinical Hospital, Federal University of Rio Grande do Sul, Porto Alegre, RS, Brazil

13 Department of Laboratory Medicine and Pathobiology, University of Toronto, Toronto, ON, Canada

14 Department of Surgery, University of Toronto, Toronto, ON, Canada

15 Texas Children's Cancer and Hematology Center, Houston, TX, USA

16 Department of Pediatrics - Hematology/Oncology, Baylor College of Medicine, Houston, TX, USA

17 Department of Neurosurgery, Baylor College of Medicine, Houston, TX, USA

18 Department of Neurosurgery, Texas Children's Hospital, Houston, TX, USA

19 Dan L Duncan Comprehensive Cancer Center, Baylor College of Medicine, Houston, TX, USA

[20] Hematology-Oncology Section, Texas Children's Cancer Center, Houston, TX, USA

[21] Department of Pharmacology, Institute for Basic Health Sciences, Federal University of Rio Grande do Sul, Porto Alegre, RS, Brazil.

Correspondence:

Natalia Hogetop Freire

nfreire@hcpa.edu.br

Rafael Roesler

rafaelroesler@hcpa.edu.br

Abstract

Changes in epigenetic processes such as histone acetylation are proposed as key events influencing cancer cell function and the initiation and progression of pediatric brain tumors. Valproic acid (VPA) is an antiepileptic drug that acts partially by inhibiting histone deacetylases (HDACs) and could be repurposed as an epigenetic anticancer therapy. Here, we show that VPA reduced medulloblastoma (MB) cell viability and led to cell cycle arrest. These effects were accompanied by enhanced H3K9 histone acetylation (H3K9ac) and decreased expression of the *MYC* oncogene. VPA impaired the expansion of MB neurospheres enriched in stemness markers, and reduced *MYC* while increasing *TP53* expression in these spheres. In addition, VPA induced morphological changes consistent with neuronal differentiation and increased expression of differentiation marker genes *TUBB3* and *ENO2*. Expression of stemness genes *SOX2*, *NES*, and *PRTG* was differentially affected by VPA in MB cells with different *TP53* status. VPA increased H3K9 occupancy of the promoter region of *TP53*. Among genes regulated by VPA, stemness regulators *MYC* and *NES* showed association with patient survival in specific MB subgroups. Our results indicate that VPA may exert antitumor effects in MB by influencing histone acetylation, which may result in modulation of stemness, neuronal differentiation, and expression of genes associated with patient prognosis in specific molecular subgroups. Importantly, the actions of VPA in MB cells and neurospheres include a reduction in expression of *MYC* and increase in *TP53*.

Keywords Valproic acid • *MYC* • *TP53* • Stemness • Differentiation • Medulloblastoma

Introduction

Medulloblastoma (MB) is the most common malignant childhood brain tumor. MB arises from neural stem cells (NSCs) or cerebellar granule neuron precursors (GNPs) that undergo genetic and epigenetic alterations [1-4]. Genomic, epigenomic, and transcriptional analyses have shown that MB is a heterogeneous disease with a variety of molecular, clinical, and prognosis features. Current classification establishes that MB comprises four distinct molecular subgroups: WNT-activated, SHH-activated, and non-WNT/non-SHH MB that includes group 3 and group 4 MB, which have a particularly poor prognosis [3-7]. Within the SHH subgroup, *TP53* status is crucial, with tumors harboring *TP53* mutations defining a particularly high-risk group of patients. *TP53* mutations are commonly associated with downstream changes including amplification of the *MYC* paralog *MYCN* [8]. *MYC* is an oncogene frequently amplified or overexpressed in many cancer types, resulting in increased cell proliferation [9].

Despite advancements in therapies in the past few decades, metastatic and recurrent MB tumors remain a challenge. Relapsed MB occurs in approximately 30% of patients and have high mortality rates [3, 4, 10]. A subpopulation of cells, known as cancer stem cells (CSCs), contributes to resistance to treatment and metastasis occurrence [11-13]. CSCs display stem cell features such as self-renewal and differentiation potential. Neurospheres derived from MB tumors or cell lines express markers related to neural progenitors and stem cells such as CD133, SOX2, and BMI-1 proto-oncogene, polycomb ring finger (BMI-1) [14]. Moreover, CD133 positive (CD133+) MB cells

are able to initiate tumors similar to those of the patient's original ones when implanted in NOD-SCID mice [11, 15], supporting the view that CSCs contribute to MB carcinogenesis.

Epigenetic mechanisms are major drivers in the establishment and maintenance of CSCs. Most common mutations found in cancer can be related to epigenetic regulators [16]. An altered epigenetic profile enables cellular reprogramming that contributes to an aberrant activation of stem cell pathways promoting the acquisition of uncontrolled self-renewal [17, 18]. Moreover, the choice between an undifferentiated and differentiated state can be controlled by alterations in the epigenome [19]. Valproic acid (VPA) is an anticonvulsant drug that also acts as an epigenetic modulator capable of inhibiting histone deacetylases (HDAC). VPA specifically inhibits HDAC class I and class IIa (HDAC 1–5, 7) leading to enhanced histone acetylation [20]. HDAC inhibitors show therapeutic potential in experimental MB [21-28]. VPA was shown to be associated with changes in MB cell cycle progression, senescence, and apoptosis [29]. In glioblastoma CSCs, VPA downregulates the expression of stemness genes *Prominin 1* (*PROM1*, which encodes CD133), *NANOG*, *POU Class 5 Homeobox 1* (*POU5F1*, also known as *OCT4*) and increases differentiation markers [30]. Hence, VPA may modulate the epigenome and contribute to CSC maintenance. Here, we explore the role of VPA in influencing genes related to differentiation and stemness maintenance in MB.

Materials and Methods

Cell Culture and Drug Treatment

Human MB D283 (ATCC® HTB-185™) and Daoy (ATCC® HTB-186™) cells were originally obtained from the American Type Culture Collection (ATCC, Rockville, USA). D283 (*TP53* wild-type) and Daoy (*TP53*-mutated) cells are proposed to be representative of group 3 and SHH MB, respectively [31]. Cells were maintained in Dulbecco's modified Eagle's medium (DMEM low glucose, Gibco®, Thermo Fisher Scientific, Waltham, USA) containing 10% (v/v) fetal bovine serum (FBS, Gibco), 1% (v/v) penicillin-streptomycin solution (10,000U/mL, Gibco) and 0.1% (v/v) amphotericin B (250 µg/mL; Gibco). Cells were cultured at 37°C in a humidified incubator under 5% CO_2. Experiments were conducted in exponentially growing cell cultures. VPA (CAS 1069-66-5, Santa Cruz Biotechnology, Dallas, USA) was dissolved in sterile water to a stock concentration of 0.3 M.

Cell Viability

Cells were treated with VPA (0.5, 1.0, 2.5, 5.0, 10.0, or 20.0 mM) for 48 h. MB cells were seeded at 3,000 cells/well in 96 wells plates and, after VPA exposure, cells were detached with trypsin-EDTA (Gibco) and counted in a Neubauer chamber with trypan for viability measurement. Doses of VPA were chosen based on previous *in vitro* studies using cultured MB cell lines [29, 32]. Experiments

were conducted in three biological replicates. For half maximal inhibitory concentration (IC_{50}) determination, cell viability data were fitted in a dose-response curve (Graphpad Prism v. 8.0).

Cell Cycle

To assess cell cycle distribution, MB control and VPA-treated cells were detached, centrifuged and washed with PBS twice. Cells were then resuspended in 50 µg/ml propidium iodide (Sigma-Aldrich, St. Louis, Mo., USA) in 0.1% Triton X-100 in 0.1% sodium citrate solution and incubated on ice for 15 min. The cells were analyzed by flow cytometry (Attune®, Applied Biosystems, Thermo Fisher Scientific) and 20,000 events were collected per sample.

Neurosphere Formation

A neurosphere formation assay was used as a model to expand putative CSCs on the basis of previous studies [22, 33]. To analyze the effects of VPA during sphere formation, MB cells were dissociated with trypsin-EDTA into cell suspension and seeded at 500 cells/well in 24-well plates. Agarose solution (1%) was used to overcome cell adherence. Cells were cultured in serum-free sphere-induction medium, containing DMEM/F12 supplemented with 20 ng/mL epidermal growth factor (Sigma-Aldrich, St. Louis, USA), 20 ng/ml basic fibroblast growth factor (Sigma-Aldrich), 2% B-27 supplement (Gibco), 0.5% N-2 supplement (Gibco, Life Technologies), 50 µg/ml bovine serum albumin (Sigma Aldrich), and antibiotics during 5 days as previously described [22]. Cells were

monitored daily until sphere formation. To analyze effects during sphere formation, VPA (1.0, 2.5, 5.0, 10.0, or 20.0 mM) was added at the first day of sphere formation assay and sphere size was measured after a period of 5 days. To verify VPA modulation after sphere formation, MB cells were dissociated with trypsin-EDTA into cell suspension and seeded at either 500 or 1,000 cells/well in 24-well ultra-low attachment plates (Corning®) in serum-free sphere-induction medium. After 5 days, VPA was added at a final concentration corresponding to half the IC_{50} (D283, 2.3 mM; Daoy, 2.2 mM) and sphere size and number were analyzed after 48 h. Images were taken using an inverted microscope at 5 X amplification and sphere size was measured using ImageJ (National Institutes of Health, Bethesda, USA). Experiments were conducted in three biological replicates.

Reverse Transcriptase Polymerase Chain Reaction (RT-qPCR)

Messenger RNA expression of target genes was analyzed by RT-qPCR. RNA was extracted from MB monolayer cells or spheres using ReliaPrep™ RNA Miniprep System (Promega, Madison, USA), in accordance with the manufacturer's instructions and quantified in NanoDrop (Thermo Fisher Scientific). The cDNA was obtained using the GoScript Reverse System (Promega) also according to the manufacturer's instructions. The mRNA expression levels of cyclin-dependent kinase inhibitor 1 (*CDKN1A*), *ENO2*, *NES*, *MYC*, *SOX2*, *TUBB3* and protogenin (*PRTG*) were quantified using PowerUp SYBR Green Master Mix (Applied Biosystems, Thermo Fisher Scientific). Primers used for RT-qPCR amplification were designed according to literature and are

shown in Supplementary Table 1. Expression of Actin Beta (ACTB) was measured as control.

Western Blot

MB control and VPA-treated cells were lysed with 1 X Lysis Buffer (Cell Lysis Buffer, Cell Signaling Technology, Danvers, USA), and protein was quantified using the Bradford protein assay (Bio-Rad Laboratories, Hercules, USA). For blotting, 40 µg of protein were separated by SDS-PAGE and transferred to a PVDF membrane. Membranes were blocked for 1 h (5% skim milk in TTBS) prior to overnight incubation at 4 °C with primary antibodies against p21 (1:200; Santa Cruz Biotechnology) and β-actin (1:2000; Santa Cruz Biotechnology) as loading control. Incubation of primary antibodies was followed by incubation with the secondary antibody adequate to each primary antibody for 1 h. Chemiluminescence was detected using ECL Western Blotting substrate (Pierce, Thermo Fisher Scientific) and images were obtained using iBright (Thermo Fisher Scientific). Immunodetection signals were analyzed using ImageJ (National Institutes of Health).

Immunofluorescence

Cells were seeded into coverslips treated with poly-L-lysine solution 0.01% (Sigma Aldrich), and exposed to VPA for 48 h, while spheres were moved to coverslips treated with poli-L-lysine solution 0.01% after VPA exposure. MB monolayer cells and spheres were washed with phosphate-buffered saline (PBS),

fixed with methanol for 5 min at room temperature (RT) and washed 2 x with ice cold PBS. Coverslips were incubated for 30 min at RT in blocking solution (1% of bovine serum albumin (BSA), 0.1% tween 20 in PBS) prior to incubation with primary antibodies against histone H3 lysine 9 acetylated residue (H3K9ac) (1:3000; Abcam), histone H3 (1:250; Thermo Fisher Scientific) at 4°C overnight. Coverslips were then rinsed three times with PBS and incubated with secondary fluorescent antibodies Alexa Fluor 488-conjugated goat anti-rabbit (1:1000; Abcam) and Alexa Fluor 594-conjugated anti-mouse (1:1000; Abcam) for 1 h at RT. Monolayer cells and spheres were then washed with PBS and coverslips were mounted with Flourisiheld containing DAPI (Sigma Aldrich) to counterstain the nuclei. Fluorescent monolayer cells and spheres were examined using a Leica microscope under 10 or 20 x magnification**.** Images of DAPI or H3K9ac were binarized and intensity of H3K9ac normalized to DAPI was measured using ImageJ for semi-quantitative analysis.

Chromatin Immunoprecipitation (ChIP)

D283 cells were seeded at a density of 1.5 X 10^6 cells per flask in T75 culture flasks previously coated with 1% agarose. Cells were cultured in a serum-free sphere-induction medium (8 ml per flask). Fresh medium (8 ml) was added on the third day of sphere induction. On the 5th day, the same amount of fresh media was added containing VPA at a final concentration of 2.3 mM. Three independent experiments were performed in parallel, each with four replicate flasks, which were pooled (using an equal number of cells from each independent experiment) to achieve a total of 4 X 10^6 cells, which were then used for ChIP experiments.

ChIP was performed using the Pierce Agarose ChIP kit (Thermo Fisher Scientific), following the manufacturer's instructions with modifications. Immediately after preparing cell pools, crosslinking was performed by incubating cells with 1% formaldehyde for 10 min at room temperature. Cells were subsequently incubated with glycine for 5 min at room temperature. Cells were then washed twice with ice-cold PBS (5,000 X g, 3 min) and once with ice-cold PBS containing protease inhibitors (5,000 X g, 3 min). Following cellular and nuclear membrane lysis according to the manufacturer's instructions, chromatin was fragmented with 6U of micrococcal nuclease per 2 X 10^6 cells as per the manufacturer's instructions. The IP was performed using Anti-Histone H3 (acetyl K9) antibody - ChIP Grade (Abcam, ab108123; 3µg/ 2 X 10^6 cells) overnight at 4ºC. Normal rabbit IgG (provided with the kit) was used as a negative control. The IP chromatin was recovered according to the manufacturer's instructions and stored at -80ºC until qPCR. qPCR was performed using the PowerUp SYBR Green Master Mix (Thermo Fisher) and 4 µL of IP chromatin per reaction, using a QuantStudio3 Real-Time System (Thermo Fisher Scientific). Primers targeting the promoter region of *TP53* are shown in Supplementary Table 2. Experiments were performed in quadruplicate and results are presented as % Input.

Gene Expression in MB Tumors and Patient Survival

Analyses of *MYC* and *NES* transcripts were performed in a previously described transcriptome dataset from patients with MB (Cavalli cohort, (GEO: GSE85218)) [34]. These two genes were chosen for analysis on the basis of the amount of information available in the dataset. We selected 612 MB tumor samples with

associated patient survival information, classified as follows: 113 group 3 MB samples, 264 group 4 samples, 172 SHH MB samples, and 64 WNT tumors. Expression levels were normalized using the R2 Genomics Analysis and Visualization Platform (http://r2.amc.nl). Tumors were classified into the different molecular subgroups and subtypes according to data available in the dataset. A feature of the R2 platform, namely the Kaplan Scan (KaplanScan algorithm), where an optimum survival cut-off is established based on statistical testing, was used.

Statistics

Data are shown as mean ± standard deviation (SD). Statistical analyses for cellular and molecular experiments were performed by independent Student's T-test when comparing two groups, or one-way analysis of variance (ANOVA) followed by Bonferroni post-hoc tests for multiple comparisons. Experiments were replicated at least three times; For ChIP-qPCR data, two-way ANOVA with Sidak-test was performed; *P* values under 0.05 indicated statistically significant differences. The GraphPad Prism 8 software (GraphPad Software, San Diego, USA) was used for analyses.

For gene expression analysis in tumor samples, patients were classified into high and low gene expression groupswith the "Survminer" package with 'minprop = 0.2'. To investigate differences between subgroups, we employed the Wilcoxon test and subsequently used the Dunn test. Statistical significance was assessed using the Holm-adjusted *P* value test. These analyses were conducted utilizing the 'ggstatsplot' package. Patient overall survival (OS) was analyzed

using the "Survival" package. Patient OS was measured from the day of diagnosis until death or the date of last follow-up. OS was calculated using the Kaplan–Meier estimate, with median values and long-rank statistics, with $P < 0.05$ indicating significant differences between groups.

Results

VPA Reduces MB Cell Viability

To evaluate the effects of VPA inhibition on MB cell viability, we exposed D283 and Daoy cells to different concentrations of VPA (0.5, 1.0, 2.5, 5.0, 10.0, or 20.0 mM) for 48 h, and viable cells were counted in a Neubauer chamber with trypan blue. VPA reduced viability in a dose-dependent manner (Fig. 1A). Estimated IC_{50} values showed that both cell lines presented similar sensitivities to VPA (2.3 mM for D283 and 2.2 mM for Daoy cells). In addition, an immunofluorescence assay was used to observe the association in VPA-induced impairment of viability with its capability to increase histone H3K9ac (Fig. 1B).

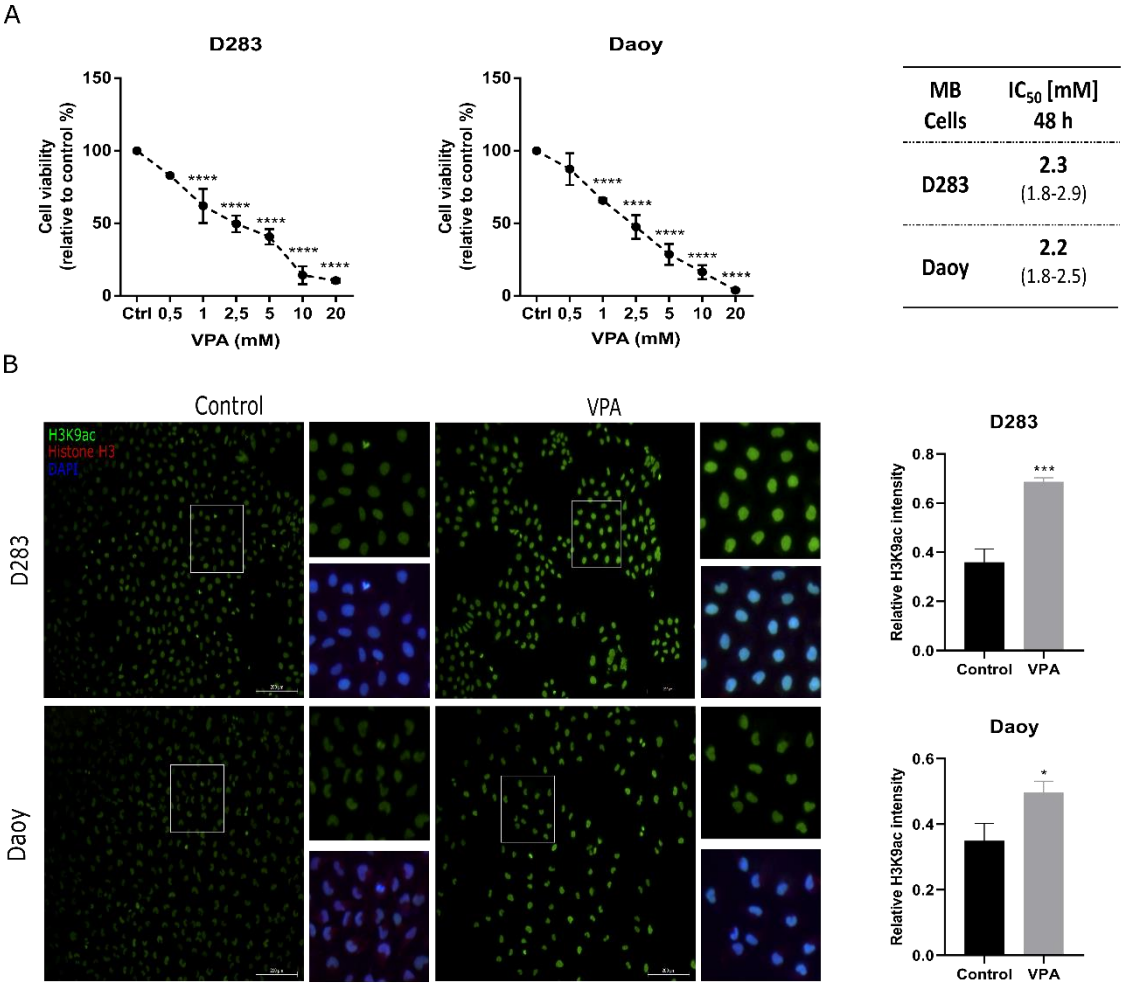

Fig 1 VPA reduces MB cell viability. **A** D283 and Daoy human MB cells were treated with a range of VPA concentrations (0.5, 1.0, 2.5, 5.0, 10.0, and 20.0 mM) for 48 h and cell viability was measured by a trypan exclusion assay. IC_{50} concentrations of VPA for MB cells with 95% confidence interval (CI) was 2.3 mM for D283 and 2.2 mM for Daoy cells. **B** Immunofluorescence assay using antibodies against H3K9ac, histone H3 and nuclei marker (DAPI) in MB control and VPA-treated cells. The IC_{50} concentration of VPA (2.3 mM for D283 and 2.2 mM for Daoy) was used. Semi-quantification of H3K9ac signal intensity relative to DAPI is shown. Results are mean ± SD of three independent experiments; * $P < 0.05$ and **** $P < 0.0001$ compared to controls.

VPA Induces Cell Cycle Arrest Accompanied by Decreased *MYC* Expression in MB Cells

We measured cell cycle distribution in MB cells after VPA exposure. Cell cycle analysis showed that VPA induced G1 arrest in Daoy cells ($P < 0.05$) (Fig. 2A). To better understand how VPA influences cell cycle progression, we examined expression of *CDKN1A*, the gene that encodes cell cycle regulator protein p21, and *MYC*, which encodes the MYC transcription factor. *CDKN1A* and *MYC* levels were not significantly altered in D283 cells. In Daoy cells, VPA was able to increase the transcriptional levels of *CDKN1A* (3.2-fold, $P < 0.05$) while reducing *MYC* (0.4-fold, $P < 0.0001$) (Fig. 2B). In addition, p21 protein levels were slightly reduced in VPA-treated D283 cells (0,22-fold, $P < 0.05$) and significantly increased in Daoy (0.97-fold, $P < 0.05$) (Fig. 2C).

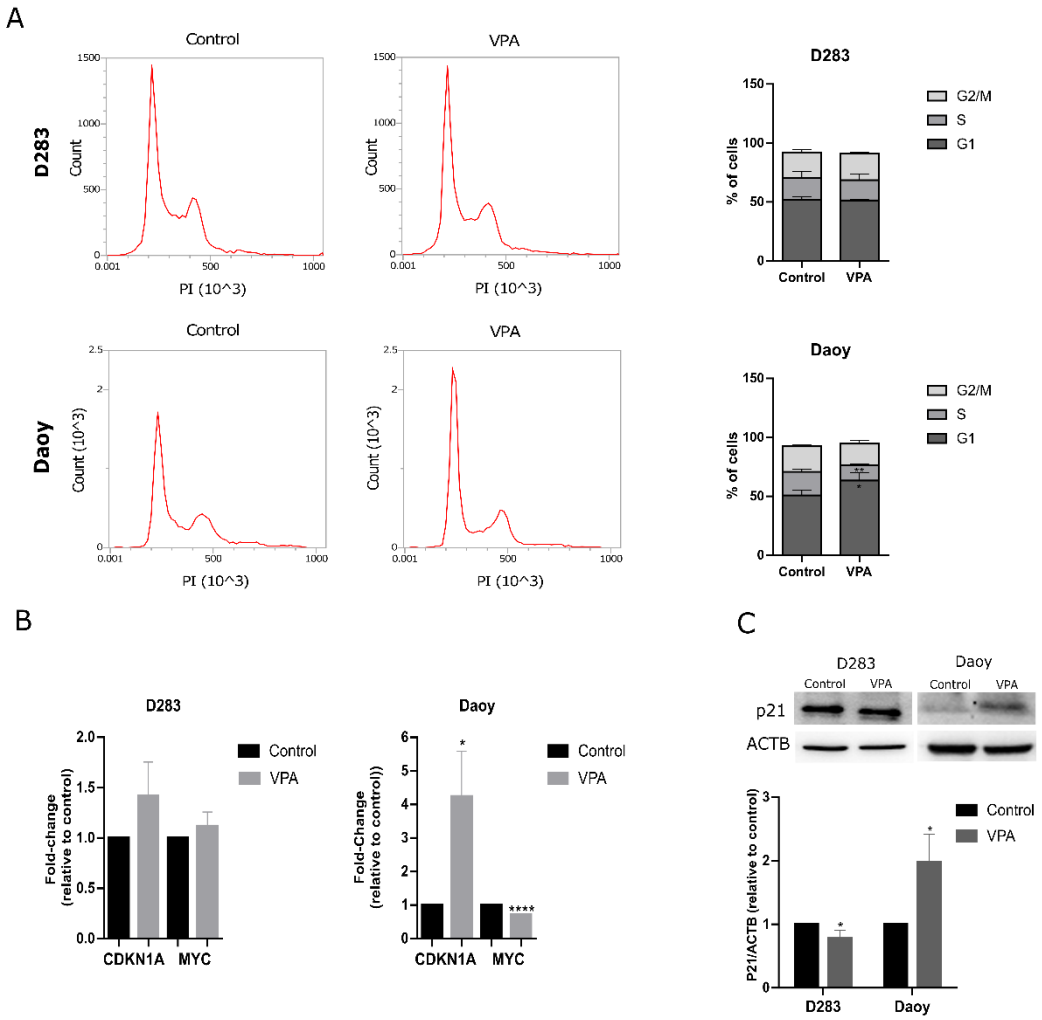

Fig 2 VPA leads to cell cycle arrest in MB cells. **A** Cell cycle analysis of D283 and Daoy cells treated with VPA and controls. **B** Relative mRNA levels of *CDKN1A* and *MYC* in MB cells were assessed using RT-qPCR. **C** Western blot analysis of the p21 protein in MB cells after VPA exposure**.** Relative Densitometric Unit (RDU) analysis normalized by β-actin and corrected by control is shown. All experiments were conducted using the IC_{50} concentration of VPA (2.3 mM for D283 and 2.2 mM for Daoy) for 48 h. Results are mean ± SD of three independent experiments; * $P < 0.05$ and **** $P < 0.0001$ compared to controls.

VPA Reduces Formation of MB Neurospheres Enriched in Stemness Genes

Sphere formation assays are widely used to expand MB CSCs [14, 22, 33, 35]. First, we verified the expression of stemness genes SOX2, *NES* and *PRTG* in D283 and Daoy spheres compared to monolayer cells. After 7 days of culturing cells in appropriated medium for expansion of MB neurospheres, D283 and Daoy-derived spheres showed an increase in transcriptional levels of both stemness genes (0.9-fold, $P < 0.01$ for *SOX2* and 2.2-fold, $P < 0.01$ for *NES* in D283; 26-fold, $P < 0.01$ for *SOX2* and 63.4-fold, $P < 0.0001$ for *NES* in Daoy). *PRTG* transcriptional levels were upregulated in D283 spheres and downregulated in Daoy spheres (1.6-fold, $P < 0.05$ in D283 spheres and 0.5-fold, $P < 0.01$ for Daoy spheres). Overall, these results suggest that the MB sphere assay enriched stemness markers (Fig. 3A, 3B).

To elucidate whether VPA could influence MB neurosphere formation, we measured sphere size after growth in the presence of VPA (1.0, 2.5, or 5.0 mM). All concentrations tested significantly reduced the sphere size after 5 days of VPA exposure compared to controls in both cell lines (Fig. 3C). We also examined whether VPA could reduce the size and number of spheres. After 5 days of sphere formation, spheres were treated with VPA (2.3 mM for D283 and 2.2 mM for Daoy) for 48 h. VPA reduced D283 sphere size by 27% ($P < 0.0001$ compared to controls) and number by 33% ($P < 0.05$ compared to controls). In Daoy VPA reduced sphere size by 25.5% ($P < 0.01$ compared to controls; Fig 3D). Immunofluorescence assay in MB spheres indicated that VPA at concentrations that impair MB sphere viability is also able to enhance H3K9ac (Fig. 3E). After VPA treatment, D283 spheres showed an increase of *SOX2* and

NES (0.7-fold, $P < 0.05$ for *SOX2* and 1.0-fold, $P < 0.01$ for *NES*) whereas *PRTG* levels were not significantly changed. In Daoy spheres, the reduction of neurosphere viability was accompanied by decrease in *SOX2* and *NES* levels (0.8-fold, $P < 0.001$ for *SOX2* and 0.8-fold, $P < 0.001$ for *NES*) (Fig. 2F).

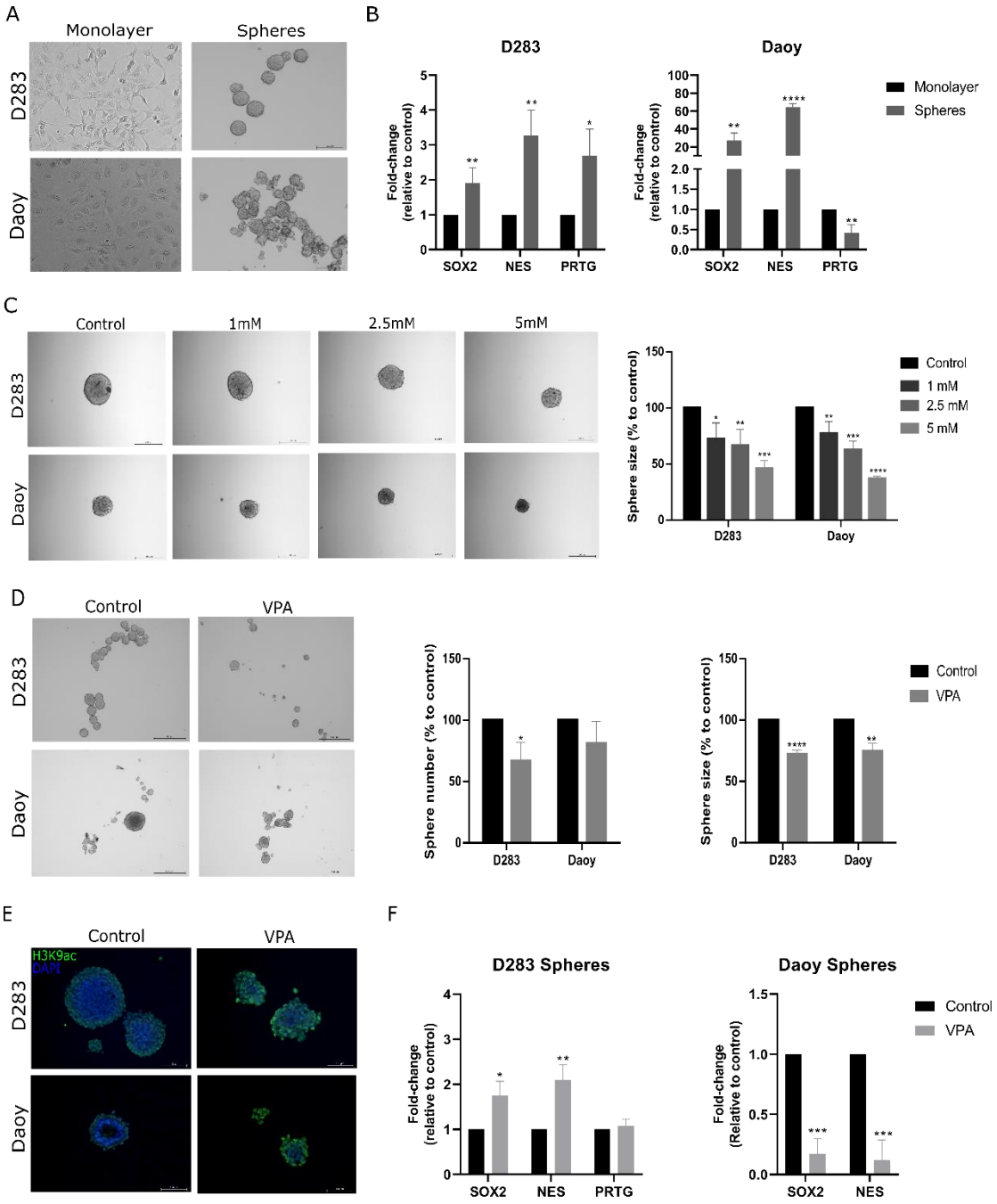

Fig 3 VPA impairs expansion of MB neurospheres enriched with stemness marker genes. **A** Representative images of D283 and Daoy MB cells and derived neurospheres. **B** Relative mRNA levels of *SOX2, NES* and *PRTG* in monolayer cells and spheres were verified using RT-qPCR. **C** VPA effects on MB sphere formation after 5 days of drug exposure. Semi-quantitative analysis of sphere size in VPA-treated and control spheres is shown. **D** After 5 days of MB neurosphere growth, VPA was added and sphere size and number were evaluated after 48 h. Semi-quantitative analyses of sphere size and number in VPA-treated and control spheres are shown. Images were taken in an inverted microscope with 5 X magnification and the scale bar corresponds to 500 µm. **E** Immunofluorescence assay against H3K9ac, histone H3 and nuclei marker (DAPI) was performed in VPA-treated and control spheres. Fluorescent images were taken in an inverted microscope with 20 X magnification and the scale bar corresponds to 100 µm. **F.** Relative mRNA levels of *SOX2*, *NES,* and *PRTG* in control and VPA-treated neurospheres were verified using RT-qPCR. Experiments were conducted using the IC_{50} concentration (2.3 mM for D283 and 2.2 mM for Daoy) of VPA. Results represent the mean ± SD of three independent experiments; * $P < 0.05$; ** $P < 0.01$; *** $P < 0.001$; and **** $P < 0.0001$ compared to controls.

VPA Reduces *MYC* and Increases *TP53* Levels in MB Neurospheres

VPA increased *CDKN1A* levels in MB neurospheres (0.9-fold, $P < 0.05$ in D283 and 6-fold, $P < 0.0001$ in Daoy-derived spheres) and decreased *MYC* levels in both D283 (0.3-fold, $P < 0.05$) and Daoy spheres (0.8-fold, $P < 0.01$) (Fig. 4A). In

D283 spheres, VPA also increased *TP53* levels (19-fold, $P < 0.01$) (Fig. 4B) Moreover, ChIP-qPCR results indicated that *CDKN1A* and *TP53* may be epigenetically modulated by VPA in D283 spheres (Fig 4C).

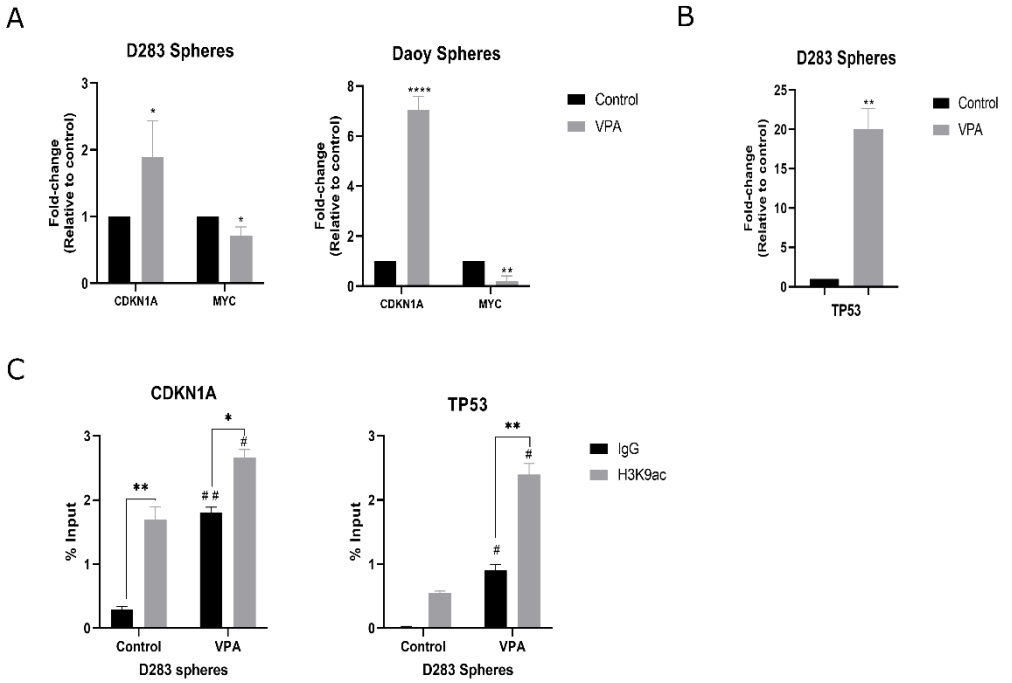

Fig 4 VPA increases CDKN1A and TP53 while reducing MYC in MB-derived neurospheres. **A-B** Relative mRNA levels of *CDKN1A*, *MYC and TP53* in MB neurospheres were verified using RT-qPCR. **C** ChIP-qPCR for the promoter region of *CDKN1A* and *TP53* in D283-derived spheres. Experiments were conducted using the IC_{50} concentration (2.3 mM for D283 and 2.2 mM for Daoy) of VPA for 48 h. Results are mean ± SD of three independent experiments; * $P < 0.05$, ** $P < 0.01$, and **** $P < 0.0001$ compared to controls. For ChIP results * $P < 0.05$ and ** $P < 0.01$ comparing VPA-treated cells versus controls immunoprecipitated with anti-IgG or anti-H3K9ac; # $P < 0.05$ comparing samples

immunoprecipitated with the same antibody (IgG versus H3K9ac) between VPA-treated and control groups.

Neuronal Differentiation and Changes in Stemness Markers Promoted by VPA in MB Cells

Exposure to VPA was accompanied by morphological changes consistent with differentiation in MB cells (Fig. 5A). We measured transcriptional levels of neuronal differentiation markers *TUBB3* and *ENO2* and found that VPA increased expression of both markers in D283 (4.6-fold, $P < 0.01$ for *TUBB3* and 1.5-fold, $P < 0.01$ for *ENO2*) and Daoy cells (0.4-fold, $P < 0.01$ for *TUBB3* and 1-fold, $P < 0.01$ in *ENO2*; Fig. 5B). In MB-derived neurospheres, VPA also increased both markers (D283-derived spheres, 1.9-fold, $P < 0.0001$ for *TUBB3* and 2-fold, $P < 0.001$ for *ENO2*; Daoy-derived spheres, 6.1-fold, $P < 0.01$ for *TUBB3* and 12.1-fold, $P < 0.01$ for *ENO2*; Fig. 5D). Immunofluorescence was used to detect beta III tubulin protein levels after VPA exposure in MB monolayer cells and neurospheres (Fig. 5C, 5E).

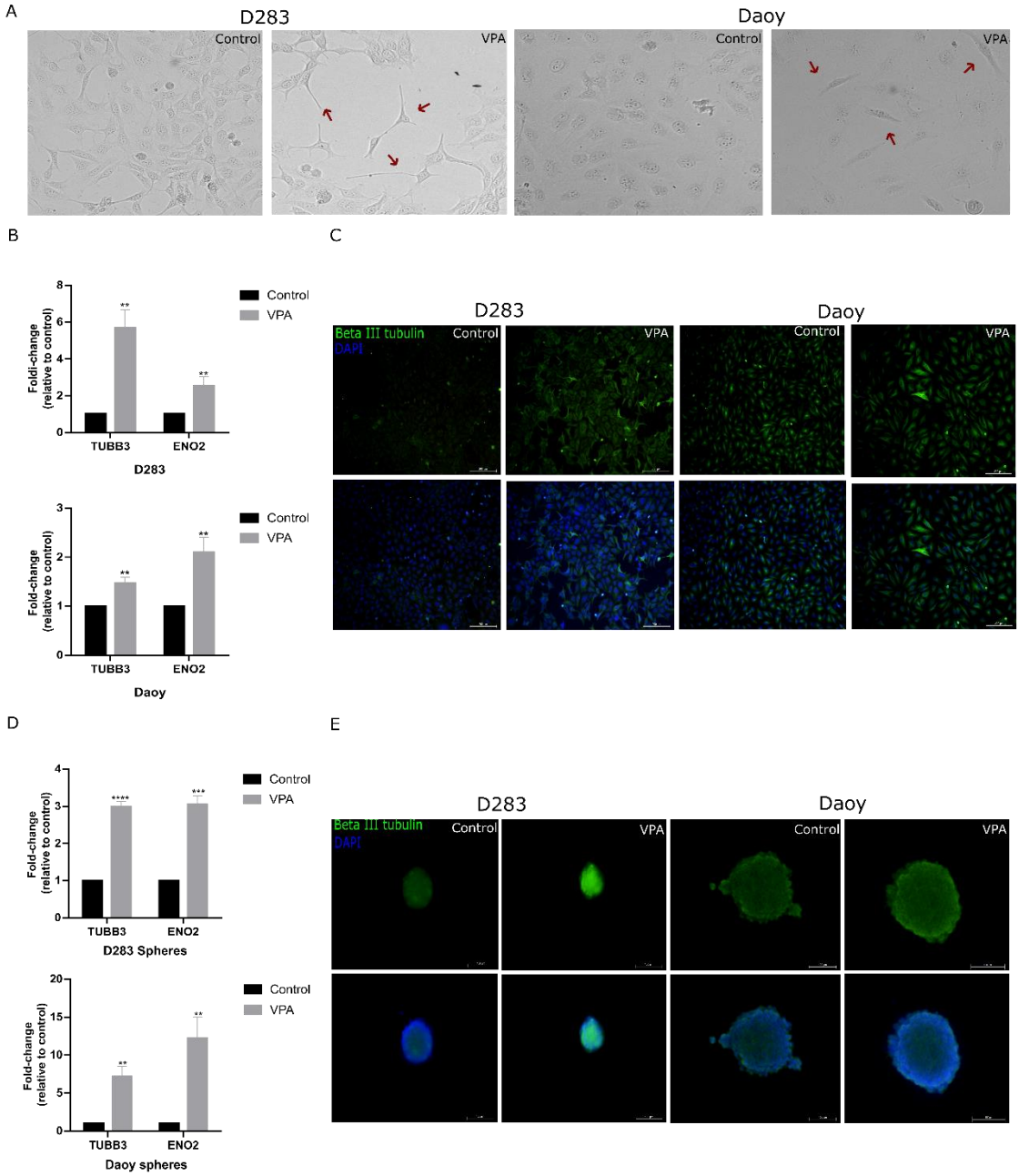

Fig 5 VPA effects on features of neuronal differentiation in MB cells. **A** Representative images of morphological changes in VPA-treated and control D283 and Daoy MB cells. **B** Relative mRNA levels of *TUBB3* and *ENO2* in MB cells were verified using RT-qPCR. **C** Immunofluorescence assay against neuronal differentiation marker protein beta III tubulin and nuclei marker (DAPI). **D** Relative mRNA levels of *TUBB3* and *ENO2* in VPA-treated and control

neurospheres derived from either D283 or Daoy cells were measured using RT-qPCR. **E** Immunofluorescence assay against neuronal differentiation marker beta III tubulin and nuclei marker (DAPI) in VPA-treated and control neurospheres. The IC_{50} concentration of VPA (2.3 mM for D283 and 2.2 mM for Daoy) was used for treatment. Fluorescent images were taken in an inverted microscope with a magnification of 10 X (monolayer) or 20 X (neurospheres). Results are mean ± SD of three independent experiments; ** $P < 0.01$, *** $P < 0.001$, and **** $P < 0.0001$ compared to controls.

Analysis of MB tumors from patients for expression of VPA-regulated stemness-regulating genes showed that expression of *MYC* in group 3 and WNT MB was significantly higher when compared to the group 4 and SHH molecular subgroups (Supplementary Fig. S1A). High levels of *MYC* transcripts were associated with better prognosis as assessed by significantly longer OS in patients with SHH MB (Supplementary Fig. S1B) but shorter OS in group 3 and group 4 MB (Supplementary Fig. S1C, S1D). Thus, higher *MYC* expression may indicate poorer prognosis in more aggressive subgroups of MB. In addition, *NES* transcription was significantly higher in WNT MB tumors compared to all other subgroups, and it was also higher in group 4 compared to group 3 and SHH MB (Supplementary Fig. S2A). Higher NES expression was associated with worse prognosis indicated by shorter OS only in patients with SHH MB (Supplementary Fig. S2B).

Discussion

MB is a pediatric tumor type that presents high frequencies of mutations in genes encoding regulators of epigenetic processes, stemness, and differentiation [16]. The resulting cellular dysregulation is also associated with the proliferation and function of MB CSCs [36]. Modulation of the histone acetylation landscape is considered a therapeutic alternative to target stemness pathways responsible for CSC maintenance [37]. VPA is a well-known anti-convulsant drug that acts at least partially as an HDAC inhibitor [20]. Previous experimental studies in MB indicate that VPA induces antitumor effects *in vitro* and *in vivo*, alters pathways related to cell cycle progression, senescence, apoptosis, and prolongs survival rates [29, 38-43]. Here, we report that VPA displays inhibitory effects on viability of MB cell lines representative of group 3 and SHH molecular subgroups, as well as in neurospheres enriched with putative MB CSCs. The effects of VPA may be related to changes in cell cycle progression, stemness maintenance, and differentiation.

Our results indicate that VPA selectively induces cell cycle arrest in Daoy cells, and affects molecular markers associated with cell cycle arrest in both D283- and Daoy-derived neurospheres, possibly by modulating p21 and *MYC*. p21 is a negative regulator of cell cycle and *MYC* is a known modulator of p21 expression due to its ability to bind to the promoter region of *CDKN1A* and thus repress transcription [44, 45]. VPA leads to *MYC* downregulation, which could explain the increase of p21 in Daoy cells. Basal *MYC* transcriptional levels were higher in D283 than in Daoy cells (3.5-fold, $P < 0.001$, data not shown). Data

available in the Human Protein Atlas database (http://proteinatlas.org) confirms different *MYC* expression in D283 and Daoy cells [46]. Within a putative CSC context, we found downregulation of *MYC* in spheres derived from both cell lines, as well as an increase of p21 transcriptional levels after VPA treatment. These findings support the possibility that modulation of *MYC* is important in mediating cell cycle arrest.

We show that VPA increases *TP53* transcription levels in D283 spheres, possibly through mechanisms related to epigenetic modulation. *TP53* is a tumor suppressor gene estimated to be mutated in about 50% of all human cancer types, with events leading to *TP53* repression being major drivers of malignant transformation. The *TP53* product, p53 protein, is a sequence-specific DNA binding protein, with its most well-known functions being promoting cell cycle arrest and apoptosis in response to various cellular stress stimuli. The cell cycle arrest response mediated by p53 depends on its direct transcriptional activation of *CDKN1A*/p21, culminating in the transcription repression of cell cycle genes [47-50]. p53 can also repress *MYC* expression in a p21-independent manner, which is necessary for efficient p53-mediated cell cycle arrest and differentiation [51]. In addition, p53 has been implicated in developmental and cell differentiation processes [52], acting as a negative modulation of proliferation and survival in NSCs, thus potentially suppressing tissue and CSC self-renewal [53]. Together, this evidence suggests that in *TP53* wild-type, *MYC* overexpressing D283-derived neurospheres, p53-mediated mechanisms may contribute to the modulation of stemness features observed in response to VPA.

We found that VPA is capable of increasing expression of neuronal differentiation markers. Histone acetylation is a crucial process regulating neural

differentiation [54]. During nervous system development, VPA reduces cell proliferation and initiates differentiation by increasing the expression of genes including *NEUROG1*, *TUBB3* and *MAP2*. VPA but not valpromide (an amide of VPA that does not inhibit HDACs) increases neuronal differentiation markers. Moreover, in NSCs from the rat embryo hippocampus, VPA causes an increase in H3K9ac active marks at the *NEUROG1* promoter, suggesting that epigenome alterations caused by VPA allows the establishment of a more differentiated phenotype [55-57]. Given that MB has granule precursor and NSCs as possible cells of origin, it can be expected that VPA is able to induce morphological changes consistent with differentiation and promote expression of neural differentiation markers [2, 58]. Once MB cells differentiate, they lose proliferative capacity and tumorigenic potential, through processes dependent on epigenetic modulation [59].

SOX2 is associated with stemness regulation, self-renewal, pluripotency, and neural differentiation in embryonic stem cells (ESCs) [60, 61]. In MB, SOX2 protein expression is critically involved in tumor development, especially in the SHH molecular subgroup [62]. GLI1/2 are downstream factors of SHH and positively regulate SOX2 by binding to its promoter, promoting self-renewal and tumorigenesis [63]. In addition, SOX2-positive cells show lower sensitivity to chemotherapy agents [64]. Our results indicate that VPA can reduce *SOX2* and *NES* transcriptional levels in Daoy neurospheres (*TP53*-mutated, representative of SHH), while increasing these markers in D283 neurospheres (*TP53* wild-type, group 3). *NES* is a progenitor marker regulated by SOX2 [65], suggesting that VPA also affects signaling components downstream of SOX2 [66].

Expression of the protogenin protein, encoded by the *PRTG* gene, is strong during a specific developmental interval in the embryonic neural tube, defining a transition stage of neurogenesis and blocked differentiation [67]. A recent study identified *PRTG*-expressing stem cells in a perivascular niche of the embryonic hindbrain which undergo oncogenic transformation to initiate group 3 MB [68]. Our finding that *PRTG* gene transcription was enhanced after neurosphere induction in D283 but not DAOY cells supports the view that protogenin acts as a specific driver of group 3 MB.

At least two genes influenced by VPA treatment in MB cells, *MYC* and *NES*, showed distinct patterns of expression among MB tumors belonging to different molecular subgroups. We found that higher *MYC* expression is associated with worse prognosis as indicated by shorter survival, which is consistent with previous evidence showing that group 3 MB tumors harbor *MYC* amplification [4, 7, 9, 69-71] and patients with *MYC*-amplified MB have a poorer prognosis despite intensive treatment regimens [34, 71]. Importantly, class I HDAC inhibitors are effective against *MYC*-amplified MB cells [72]. We also found that higher *NES* expression was associated with shorter OS in patients with SHH MB. A high content of Nestin, the protein encoded by the *NES* gene, is a feature of MB CSCs [73] and SHH-driven cancers [74].

Together with previous studies, our results suggest that the potential of VPA in MB therapy warrants further exploration. A case of successful use of dose-dense neoadjuvant chemotherapy combined with VPA in a child with MB has been reported [75]. One important limitation, however, is that the IC_{50} we found for inhibition of MB viability is over three times higher than the plasma therapeutic concentration for VPA used in the clinical setting, and only 10 to 20%

of the plasma concentration reaches the cerebrospinal fluid (CSF). A concentration of only 0.4 mm of VPA is necessary for HDAC1 inhibition, which falls within the therapeutic range [76, 77]. A requirement for very high (and potentially toxic) doses of VPA may thus be a challenge for its repurposing as an anticancer drug to treat MB.

In conclusion, our results indicate that VPA can influence MB viability and features related to cell cycle regulation, stemness, and differentiation, possibly by increasing histone acetylation, reducing *MYC*, and increasing *TP53*. A schematic summary of key findings is shown in Fig. 6. It is possible that VPA-induced inhibition of HDAC activity and the MYC-p21-SOX2 axis influences the development and aggressiveness of MB tumors.

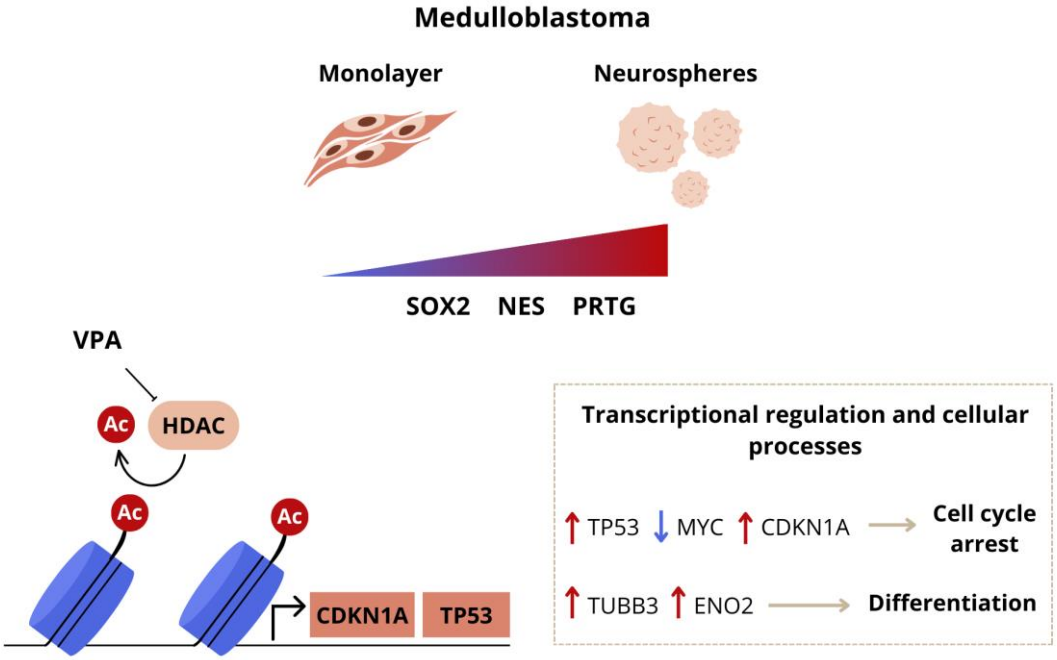

Fig 6 Schematic model highlighting selected aspects of VPA-induced molecular and functional effects in MB. Exposure to VPA leads to a reduction in MB cell cycle arrest and differentiation in MB monolayer and neurospheres. VPA can increase *TP53* while reducing *MYC* expression, potentially inhibiting stemness, and promoting features of differentiation.

Author Contribution Natália Hogetop Freire, Alice Laschuk Herlinger, Julia Vanini, Matheus Dalmolin, Marcelo A. C. Fernandes, Carolina Nör, Vijay Ramaswamy, Caroline Brunetto de Farias, André Tesainer Brunetto, Algemir Lunardi Brunetto, Lauro José Gregianin, Mariane da Cunha Jaeger, Michael D. Taylor, and Rafael Roesler contributed to the study conception and design and data interpretation. Material preparation, data collection and analysis were performed by Natália Hogetop Freire, Alice Laschuk Herlinger, Julia Vanini, and Matheus Dalmolin. The first draft of the manuscript was written by Natália Hogetop Freire. Natália Hogetop Freire, Alice Laschuk Herlinger, Julia Vanini, Matheus Dalmolin, Marcelo A. C. Fernandes, Carolina Nör, Vijay Ramaswamy, Caroline Brunetto de Farias, André Tesainer Brunetto, Algemir Lunardi Brunetto, Lauro José Gregianin, Mariane da Cunha Jaeger, Michael D. Taylor, and Rafael Roesler revised previous versions of the manuscript, read and approved the final manuscript.

Funding This work was supported by the National Council for Scientific and Technological Development (CNPq, MCTI, Brazil) grant numbers 305647/2019-9, 405608/2021-7, and 406484/2022-8 (INCT BioOncoPed) to R.R.,

101566/2022-0 to A.L.H, and scholarship to N.H.F., Ministry of Health/CNPq/FAPERGS PPSUS grant number 21/2551-0000114-3 to R.R. and L.G., the Children's Cancer Institute (ICI), and Clinical Hospital (HCPA) institutional research fund grant numbers 2020-0069 and 2023-0021 to R.R. C.N. is supported by a William Donald Nash Brain Tumour Research Fellowship, Brain Tumour Foundation of Canada, and the Swifty Foundation. V.R. is supported by operating funds from the Canadian Institutes for Health Research, the Garron Family Cancer Centre, the C.R. Younger Foundation, the Canadian Cancer Society Research Institute, Brain Canada, the Rally Foundation for Childhood Cancer, and a Canada Research Chair in Pediatric Neuro-Oncology. M.D.T. is a CPRIT Scholar in Cancer Research (CPRIT - RR220051) and the Cyvia and Melvyn Wolff Chair of Pediatric Neuro-Oncology, Texas Children's Cancer and Hematology Center. M.D.T. is also supported by the NIH (R01NS106155, R01CA159859, and R01CA255369), the Pediatric Brain Tumor Foundation, the Terry Fox Research Institute, the Canadian Institutes of Health Research, the Cure Search Foundation, the Matthew Larson Foundation (IronMatt), b.r.a.i.n.child, Meagan's Walk, the Swifty Foundation, the Brain Tumour Charity, Genome Canada, Genome BC, Genome Quebec, the Ontario Research Fund, Worldwide Cancer Research, the V Foundation for Cancer Research, the Ontario Institute for Cancer Research through funding provided by the Government of Ontario, a Canadian Cancer Society Research Institute Impact grant, a Cancer Research UK Brain Tumour Award, a Stand Up To Cancer (SU2C) St. Baldrick's Pediatric Dream Team Translational Research grant (SU2C-AACR-DT1113), and SU2C Canada Cancer Stem Cell Dream Team Research Funding (SU2C-AACR-DT-19-15) provided by the Government of Canada through Genome

Canada and the Canadian Institutes of Health Research, with supplementary support from the Ontario Institute for Cancer Research through funding provided by the Government of Ontario. M.D.T. was also supported by the Garron Family Chair in Childhood Cancer Research at the Hospital for Sick Children and the University of Toronto.

Data Availability The dataset analyzed in this study is available in the Gene Expression Omnibus repository, https://www.ncbi.nlm.nih.gov/geo/query/acc.cgi?acc=GSE85217. Other data can be provided upon request.

Declarations

Competing Interests The authors declare no competing interests.

Ethics Approval This work was approved by the appropriate institutional committee under number 2020-0069 (HCPA). This study did not directly involve human or animal subjects.

Consent to Participate Not applicable

Consent for Publication Not applicable

Conflict of Interest The authors declare no competing interests.

References

1. Schüller U, Heine VM, Mao J, Kho AT, Dillon AK, Han YG, Huillard E, Sun T, Ligon AH, Qian Y, Ma Q, Alvarez-Buylla A, McMahon AP, Rowitch DH, Ligon KL (2008) Acquisition of granule neuron precursor identity is a critical determinant of progenitor cell competence to form Shh-induced medulloblastoma. Cancer Cell 14(2): 123-134. https://doi.org/10.1016/j.ccr.2008.07.005

2. Pei Y, Moore CE, Wang J, Tewari AK, Eroshkin A, Cho YJ, Witt H, Korshunov A, Read TA, Sun JL, Schmitt EM, Miller CR, Buckley AF, McLendon RE, Westbrook TF, Northcott PA, Taylor MD, Pfister SM, Febbo PG, Wechsler-Reya RJ (2012) An animal model of MYC-driven medulloblastoma. Cancer Cell 21(2): 155-167. https://doi.org/10.1016/j.ccr.2011.12.021

3. Juraschka K, Taylor MD (2019) Medulloblastoma in the age of molecular subgroups: a review. J Neurosurg Pediatr 24(4): 353-363. https://doi.org/10.3171/2019.5.PEDS18381

4. Northcott PA, Robinson GW, Kratz CP, Mabbott DJ, Pomeroy SL, Clifford SC, Rutkowski S, Ellison DW, Malkin D, Taylor MD, Gajjar A, Pfister SM (2019) Medulloblastoma. Nat Rev Dis Primers 5(1): 11. https://doi.org/10.1038/s41572-019-0063-6

5. Northcott PA, Korshunov A, Pfister SM, Taylor MD (2012) The clinical implications of medulloblastoma subgroups. Nat Rev Neurol 8(6): 340-351. https://doi.org/10.1038/nrneurol.2012.78 8, 340–351

6. Taylor MD, Northcott PA, Korshunov A, Remke M, Cho YJ, Clifford SC, Eberhart CG, Parsons, DW, Rutkowski S, Gajjar A, Ellison DW, Lichter P, Gilbertson RJ, Pomeroy SL, Kool M, Pfister SM (2012) Molecular subgroups of medulloblastoma: The current consensus. Acta Neuropathol 123(4): 465–472. https://doi.org/10.1007/s00401-011-0922-z

7 Northcott PA, Buchhalter I, Morrissy AS, Hovestadt V, Weischenfeldt J, Ehrenberger T, Gröbner S, Segura-Wang M, Zichner T, Rudneva VA, Warnatz HJ, Sidiropoulos N, Phillips AH, Schumacher S, Kleinheinz K, Waszak SM, Erkek S, Jones DTW, Worst BC, Kool M, Zapatka M, Jäger N, Chavez L, Hutter B, Bieg M, Paramasivam N, Heinold M, Gu Z, Ishaque N, Jäger-Schmidt C, Imbusch CD, Jugold A, Hübschmann D, Risch T, Amstislavskiy V, Gonzalez FGR, Weber UD, Wolf S, Robinson GW, Zhou X, Wu G, Finkelstein D, Liu Y, Cavalli FMG, Luu B, Ramaswamy V, Wu X, Koster J, Ryzhova M, Cho YJ, Pomeroy SL, Herold-Mende C, Schuhmann M, Ebinger M, Liau LM, Mora J, McLendon RE, Jabado N, Kumabe T, Chuah E, Ma Y, Moore RA, Mungall AJ, Mungall KL, Thiessen N, Tse K, Wong T, Jones SJM, Witt O, Milde T, Von Deimling A, Capper D, Korshunov A, Yaspo ML, Kriwacki R, Gajjar A, Zhang J, Beroukhim R, Fraenkel E, Korbel JO, Brors B, Schlesner M, Eils R, Marra MA, Pfister SM, Taylor MD, Lichter P (2017) The whole-genome landscape of medulloblastoma subtypes. Nature 547(7663): 311-317. https://doi.org/10.1038/nature22973 311–317

8 Ramaswamy V, Nör C, Taylor MD (2015) p53 and meduloblastoma. Cold Spring Harb Perspect Med 6(2): a026278. https://doi.org/10.1101/cshperspect.a026278

9. Roussel MF, Robinson GW (2013) Role of MYC in medulloblastoma. Cold Spring Harb Perspect Med 3(11): a014308. https://doi.org/10.1101/cshperspect.a014308

10. Hill RM, Richardson S, Schwalbe EC, Hicks D, Lindsey JC, Crosier S, Rafiee G, Grabovska Y, Wharton SB, Jacques TS, Michalski A, Joshi A, Pizer B, Williamson D, Bailey S, Clifford SC (2020) Time, pattern, and outcome of medulloblastoma relapse and their association with tumour biology at diagnosis and therapy: a multicentre cohort study. Lancet Child Adolesc Health 4(12): 865-874. https://doi.org/10.1016/S2352-4642(20)30246-7

11. Fan X, Eberhart CG (2008) Medulloblastoma stem cells. J Clin Oncol 26(17): 2821-2827. https://doi.org/10.1200/JCO.2007.15.2264

12. Manoranjan B, Venugopal C, McFarlane N, Doble BW, Dunn SE, Scheinemann K, Singh SK (2013) Medulloblastoma stem cells: modeling tumor heterogeneity. Cancer Lett 338(1): 23-31. https://doi.org/10.1016/j.canlet.2012.07.010

13. Manoranjan B, Wang X, Hallett RM, Venugopal C, Mack SC, McFarlane N, Nolte SM, Scheinemann K, Gunnarsson T, Hassell JA, Taylor MD, Lee C, Triscott J, Foster CM, Dunham C, Hawkins C, Dunn SE, Singh SK (2013) FoxG1 interacts with Bmi1 to regulate self-renewal and tumorigenicity of

medulloblastoma stem cells. Stem Cells 31(7): 1266-1277. https://doi.org/10.1002/stem.1401

14. Hemmati HD, Nakano I, Lazareff JA, Masterman-Smith M, Geschwind DH, Bronner-Fraser M, Kornblum HI (2003) Cancerous stem cells can arise from pediatric brain tumors. Proc Natl Acad Sci U S A 100(25): 15178-15183. https://doi.org/10.1073/pnas.2036535100

15. Singh SK, Hawkins C, Clarke ID, Squire JA, Bayani J, Hide T, Henkelman RM, Cusimano MD, Dirks PB (2004) Identification of human brain tumour initiating cells. Nature 432(7015): 396-401. https://doi.org/10.1038/nature03128

16. Huether R, Dong L, Chen X, Wu G, Parker M, Wei L, Ma J, Edmonson MN, Hedlund EK, Rusch MC, Shurtleff SA, Mulder HL, Boggs K, Vadordaria B, Cheng J, Yergeau D, Song G, Becksfort J, Lemmon G, Weber C, Cai Z, Dang J, Walsh M, Gedman AL, Faber Z, Easton J, Gruber T, Kriwacki RW, Partridge JF, Ding L, Wilson RK, Mardis ER, Mullighan CG, Gilbertson RJ, Baker SJ, Zambetti G, Ellison DW, Zhang J, Downing JR (2014) The landscape of somatic mutations in epigenetic regulators across 1,000 paediatric cancer genomes. Nat Commun 5: 3630. https://doi.org/10.1038/ncomms4630

17. Jagani Z, Mora-Blanco EL, Sansam CG, McKenna ES, Wilson B, Chen D, Klekota J, Tamayo P, Nguyen PT, Tolstorukov M, Park PJ, Cho YJ, Hsiao K, Buonamici S, Pomeroy SL, Mesirov JP, Ruffner H, Bouwmeester T, Luchansky SJ, Murtie J, Kelleher JF, Warmuth M, Sellers WR, Roberts CW, Dorsch M (2010) Loss of the tumor suppressor Snf5 leads to aberrant

activation of the Hedgehog-Gli pathway. Nat Med 16(12): 1429-1433. https://doi.org/10.1038/nm.2251

18. Oleksiewicz U, Gładych M, Raman AT, Heyn H, Mereu E, Chlebanowska P, Andrzejewska A, Sozańska B, Samant N, Fąk K, Auguścik P, Kosiński M, Wróblewska JP, Tomczak K, Kulcenty K, Płoski R, Biecek P, Esteller M, Shah PK, Rai K, Wiznerowicz M (2017) TRIM28 and interacting KRAB-ZNFs control self-renewal of human pluripotent stem cells through epigenetic repression of pro-differentiation genes. Stem Cell Reports 9(6): 2065-2080. https://doi.org/10.1016/j.stemcr.2017.10.031

19. Wainwright EN, Scaffidi P (2017) Epigenetics and cancer stem cells: unleashing, hijacking, and restricting cellular plasticity. Trends Cancer 3(5): 372-386. https://doi.org/10.1016/j.trecan.2017.04.004

20. Chateauvieux S, Morceau F, Dicato M, Diederich M (2010) Molecular and therapeutic potential and toxicity of valproic acid. J Biomed Biotechnol 2010: 479364. https://doi.org/10.1155/2010/479364

21. Nör C, de Farias CB, Abujamra AL, Schwartsmann G, Brunetto AL, Roesler R (2011) The histone deacetylase inhibitor sodium butyrate in combination with brain-derived neurotrophic factor reduces the viability of DAOY human medulloblastoma cells. Childs Nerv Syst 27(6): 897-901. https://doi.org/10.1007/s00381-011-1439-4

22. Nör C, Sassi FA, de Farias CB, Schwartsmann G, Abujamra AL, Lenz G, Brunetto AL, Roesler R (2013) The histone deacetylase inhibitor sodium butyrate promotes cell death and differentiation and reduces neurosphere

formation in human medulloblastoma cells. Mol Neurobiol 48(3): 533-543. https://doi.org/10.1007/s12035-013-8441-7

23. Jaeger M, Ghisleni EC, Fratini L, Brunetto AL, Gregianin LJ, Brunetto AT, Schwartsmann G, de Farias CB, Roesler R (2016) Viability of D283 medulloblastoma cells treated with a histone deacetylase inhibitor combined with bombesin receptor antagonists. Childs Nerv Syst 32(1): 61-64. https://doi.org/10.1007/s00381-015-2963-4

24. Perla AS, Fratini L, Cardoso PS, de Farias CB, da Cunha Jaeger M, Roesler R (2020) Fingolimod (FTY720) reduces viability and survival and increases histone H3 acetylation in medulloblastoma cells. Pediatr Hematol Oncol 37(2): 170-175. https://doi.org/10.1080/08880018.2019.1699213

25. da Cunha Jaeger M, Ghisleni EC, Cardoso PS, Siniglaglia M, Falcon T, Brunetto AT, Brunetto AL, de Farias CB, Taylor MD, Nör C, Ramaswamy V, Roesler R (2020) HDAC and MAPK/ERK inhibitors cooperate to reduce viability and stemness in medulloblastoma. J Mol Neurosci 70(6): 981-992. https://doi.org/10.1007/s12031-020-01505-y

26. Perla A, Fratini L, Cardoso PS, Nör C, Brunetto AT, Brunetto AL, de Farias CB, Jaeger M, Roesler R (2020) Histone deacetylase inhibitors in pediatric brain cancers: biological activities and therapeutic potential. Front Cell Dev Biol 8: 546. https://doi.org/10.3389/fcell.2020.00546

27. Freire NH, Jaeger MDC, de Farias CB, Nör C, Souza BK, Gregianin L, Brunetto AT, Roesler R (2023) Targeting the epigenome of cancer stem cells in pediatric nervous system tumors. Mol Cell Biochem 478(10): 2241-2255. https://doi.org/10.1007/s11010-022-04655-2

28. Laschuk Herlinger A, Lovatto Michaelsen G, Sinigaglia M, Fratini L, Nogueira Debom G, Braganhol E, Brunetto de Farias C, Lunardi Brunetto A, Tesainer Brunetto A, da Cunha Jaeger M, Roesler R (2023) Modulation of viability, proliferation, and stemness by rosmarinic acid in medulloblastoma cells: involvement of HDACs and EGFR. Neuromolecular Med 25(4): 573-585. https://doi.org/10.1007/s12017-023-08758-x

29. Li XN, Shu Q, Su JM, Perlaky L, Blaney SM, Lau CC (2005) Valproic acid induces growth arrest, apoptosis, and senescence in medulloblastomas by increasing histone hyperacetylation and regulating expression of p21Cip1, CDK4, and CMYC. Mol Cancer Ther 4(12): 1912-1922. https://doi.org/10.1158/1535-7163.MCT-05-0184

30. Alvarez AA, Field M, Bushnev S, Longo MS, Sugaya K (2015) The effects of histone deacetylase inhibitors on glioblastoma-derived stem cells. J Mol Neurosci 55(1): 7-20. https://doi.org/10.1007/s12031-014-0329-0

31. Ivanov DP, Coyle B, Walker DA, Grabowska AM (2016) In vitro models of medulloblastoma: choosing the right tool for the job. J Biotechnol 236: 10-25. https://doi.org/10.1016/j.jbiotec.2016.07.028

32. Riva G, Cilibrasi C, Bazzoni R, Cadamuro M, Negroni C, Butta V, Strazzabosco M, Dalprà L, Lavitrano M, Bentivegna A (2018) Valproic acid inhibits proliferation and reduces invasiveness in glioma stem cells through Wnt/β catenin signalling activation. Genes (Basel) 9(11): 522. https://doi.org/10.3390/genes9110522

33. S Franco S, Szczesna K, Iliou MS, Al-Qahtani M, Mobasheri A, Kobolák J, Dinnyés A (2016) In vitro models of cancer stem cells and clinical

applications. BMC Cancer 16(Suppl 2): 738. https://doi.org/10.1186/s12885-016-2774-3

34. Cavalli FMG, Remke M, Rampasek L, Peacock J, Shih DJH, Luu B, Garzia L, Torchia J, Nor C, Morrissy AS, Agnihotri S, Thompson YY, Kuzan-Fischer CM, Farooq H, Isaev K, Daniels C, Cho BK, Kim SK, Wang KC, Lee JY, Grajkowska WA, Perek-Polnik M, Vasiljevic A, Faure-Conter C, Jouvet A, Giannini C, Nageswara Rao AA, Li KKW, Ng HK, Eberhart CG, Pollack IF, Hamilton RL, Gillespie GY, Olson JM, Leary S, Weiss WA, Lach B, Chambless LB, Thompson RC, Cooper MK, Vibhakar R, Hauser P, van Veelen MC, Kros JM, French PJ, Ra YS, Kumabe T, López-Aguilar E, Zitterbart K, Sterba J, Finocchiaro G, Massimino M, Van Meir EG, Osuka S, Shofuda T, Klekner A, Zollo M, Leonard JR, Rubin JB, Jabado N, Albrecht S, Mora J, Van Meter TE, Jung S, Moore AS, Hallahan AR, Chan JA, Tirapelli DPC, Carlotti CG, Fouladi M, Pimentel J, Faria CC, Saad AG, Massimi L, Liau LM, Wheeler H, Nakamura H, Elbabaa SK, Perezpeña-Diazconti M, Chico Ponce de León F, Robinson S, Zapotocky M, Lassaletta A, Huang A, Hawkins CE, Tabori U, Bouffet E, Bartels U, Dirks PB, Rutka JT, Bader GD, Reimand J, Goldenberg A, Ramaswamy V, Taylor MD (2017) Intertumoral heterogeneity within medulloblastoma subgroups. Cancer Cell 31(6): 737-754.e6. https://doi.org/10.1016/j.ccell.2017.05.005

35. Singec I, Knoth R, Meyer RP, Maciaczyk J, Volk B, Nikkhah G, Frotscher M, Snyder EY (2006) Defining the actual sensitivity and specificity of the neurosphere assay in stem cell biology. Nat Methods 3(10): 801-806. https://doi.org/10.1038/nmeth926

36. Paik S, Maule F, Gallo M (2021) Dysregulation of chromatin organization in pediatric and adult brain tumors: oncoepigenomic contributions to tumorigenesis and cancer stem cell properties. Genome 64(4): 326-336. https://doi.org/10.1139/gen-2020-0097

37. Liu N, Li S, Wu N, Cho KS (2017) Acetylation and deacetylation in cancer stem-like cells. Oncotarget 8(51): 89315-89325. https://doi.org/10.18632/oncotarget.19167

38. Shu Q, Antalffy B, Su JM, Adesina A, Ou CN, Pietsch T, Blaney SM, Lau CC, Li XN (2006) Valproic Acid prolongs survival time of severe combined immunodeficient mice bearing intracerebellar orthotopic medulloblastoma xenografts. Clin Cancer Res 12(15): 4687-4694. https://doi.org/10.1158/1078-0432.CCR-05-2849

39. Ecke I, Petry F, Rosenberger A, Tauber S, Mönkemeyer S, Hess I, Dullin C, Kimmina S, Pirngruber J, Johnsen SA, Uhmann A, Nitzki F, Wojnowski L, Schulz-Schaeffer W, Witt O, Hahn H (2009) Antitumor effects of a combined 5-aza-2'deoxycytidine and valproic acid treatment on rhabdomyosarcoma and medulloblastoma in Ptch mutant mice. Cancer Res 69(3): 887-895. https://doi.org/10.1158/0008-5472.CAN-08-0946

40. Häcker S, Karl S, Mader I, Cristofanon S, Schweitzer T, Krauss J, Rutkowski S, Debatin KM, Fulda S (2011) Histone deacetylase inhibitors prime medulloblastoma cells for chemotherapy-induced apoptosis by enhancing p53-dependent Bax activation. Oncogene 30(19): 2275-2281. https://doi.org/10.1038/onc.2010.599

41 Patties I, Kortmann RD, Glasow A. Inhibitory effects of epigenetic modulators and differentiation inducers on human medulloblastoma cell lines (2013) J Exp Clin Cancer Res 32(1): 27. https://doi.org/10.1186/1756-9966-32-27

42 Patties I, Kortmann RD, Menzel F, Glasow A (2016) Enhanced inhibition of clonogenic survival of human medulloblastoma cells by multimodal treatment with ionizing irradiation, epigenetic modifiers, and differentiation-inducing drugs. J Exp Clin Cancer Res 35(1): 94. https://doi.org/10.1186/s13046-016-0376-1

43 Mascaro-Cordeiro B, Oliveira ID, Tesser-Gamba F, Pavon LF, Saba-Silva N, Cavalheiro S, Dastoli P, Toledo SRC (2018) Valproic acid treatment response in vitro is determined by TP53 status in medulloblastoma. Childs Nerv Syst 34(8): 1497-1509. https://doi.org/10.1007/s00381-018-3817-7

44. Claassen GF, Hann SR (2000) A role for transcriptional repression of p21CIP1 by c-Myc in overcoming transforming growth factor beta -induced cell-cycle arrest. Proc Natl Acad Sci U S A 97(17): 9498-9503. https://doi.org/10.1073/pnas.150006697

45. Gartel AL, Ye X, Goufman E, Shianov P, Hay N, Najmabadi F, Tyner AL (2001) Myc represses the p21(WAF1/CIP1) promoter and interacts with Sp1/Sp3. Proc Natl Acad Sci U S A 98(8): 4510-4515. https://doi.org/10.1073/pnas.081074898

46. Uhlen M, Zhang C, Lee S, Sjöstedt E, Fagerberg L, Bidkhori G, Benfeitas R, Arif M, Liu Z, Edfors F, Sanli K, von Feilitzen K, Oksvold P, Lundberg E, Hober S, Nilsson P, Mattsson J, Schwenk JM, Brunnström H, Glimelius B,

Sjöblom T, Edqvist PH, Djureinovic D, Micke P, Lindskog C, Mardinoglu A, Ponten F (2017) A pathology atlas of the human cancer transcriptome. Science 357(6352): eaan2507. https://doi.org/10.1126/science.aan2507

47. el-Deiry WS, Tokino T, Velculescu VE, Levy DB, Parsons R, Trent JM, Lin D, Mercer WE, Kinzler KW, Vogelstein B (1993) WAF1, a potential mediator of p53 tumor suppression. Cell 75(4): 817-825. https://doi.org/10.1016/0092-8674(93)90500-p

48. Abbas T, Dutta A (2009) p21 in cancer: intricate networks and multiple activities. Nat Rev Cancer 9(6): 400-414. https://doi.org/10.1038/nrc2657

49. Quaas M, Müller GA, Engeland K (2012) p53 can repress transcription of cell cycle genes through a p21(WAF1/CIP1)-dependent switch from MMB to DREAM protein complex binding at CHR promoter elements. Cell Cycle 11(24): 4661-4672. https://doi.org/10.4161/cc.22917

50. Engeland K (2018) Cell cycle arrest through indirect transcriptional repression by p53: I have a DREAM. Cell Death Differ 25(1): 114-132. https://doi.org/10.1038/cdd.2017.172

51. Ho JS, Ma W, Mao DY, Benchimol S (2005) p53-Dependent transcriptional repression of c-myc is required for G1 cell cycle arrest. Mol Cell Biol 25(17): 7423-7431. https://doi.org/10.1128/MCB.25.17.7423-7431.2005

52. Jain AK, Barton MC (2018) p53: emerging roles in stem cells, development and beyond. Development 145(8): dev158360. https://doi.org/10.1242/dev.158360

53. Meletis K, Wirta V, Hede SM, Nistér M, Lundeberg J, Frisén J (2006) p53 suppresses the self-renewal of adult neural stem cells. Development 133(2): 363-369. https://doi.org/10.1242/dev.02208

54. Nothof SA, Magdinier F, Van-Gils J (2022) Chromatin structure and dynamics: focus on neuronal differentiation and pathological implication. Genes (Basel) 13(4): 639. https://doi.org/10.3390/genes13040639

55. Yu IT, Park JY, Kim SH, Lee JS, Kim YS, Son H (2009) Valproic acid promotes neuronal differentiation by induction of proneural factors in association with H4 acetylation. Neuropharmacology 56(2): 473-480. https://doi.org/10.1016/j.neuropharm.2008.09.019

56. Zhang X, He X, Li Q, Kong X, Ou Z, Zhang L, Gong Z, Long D, Li J, Zhang M, Ji W, Zhang W, Xu L, Xuan A (2017) PI3K/AKT/mTOR signaling mediates valproic acid-induced neuronal differentiation of neural stem cells through epigenetic modifications. Stem Cell Reports 8(5): 1256-1269. https://doi.org/10.1016/j.stemcr.2017.04.006

57. Fernandes S, Vinnakota R, Kumar J, Kale V, Limaye L (2019) Improved neural differentiation of normal and abnormal induced pluripotent stem cell lines in the presence of valproic acid. J Tissue Eng Regen Med 13(8): 1482-1496. https://doi.org/10.1002/term.2904

58. Schüller U, Heine VM, Mao J, Kho AT, Dillon AK, Han YG, Huillard E, Sun T, Ligon AH, Qian Y, Ma Q, Alvarez-Buylla A, McMahon AP, Rowitch DH, Ligon KL (2008) Acquisition of granule neuron precursor identity is a critical determinant of progenitor cell competence to form Shh-induced

medulloblastoma. Cancer Cell 14(2): 123-134. https://doi.org/10.1016/j.ccr.2008.07.005

59. Cheng Y, Liao S, Xu G, Hu J, Guo D, Du F, Contreras A, Cai KQ, Peri S, Wang Y, Corney DC, Noronha AM, Chau LQ, Zhou G, Wiest DL, Bellacosa A, Wechsler-Reya RJ, Zhao Y, Yang ZJ (2020) NeuroD1 dictates tumor cell differentiation in medulloblastoma. Cell Rep 31(12): 107782. https://doi.org/10.1016/j.celrep.2020.107782

60. Masui S, Nakatake Y, Toyooka Y, Shimosato D, Yagi R, Takahashi K, Okochi H, Okuda A, Matoba R, Sharov AA, Ko MS, Niwa H (2007) Pluripotency governed by Sox2 via regulation of Oct3/4 expression in mouse embryonic stem cells. Nat Cell Biol 9(6): 625-635. https://doi.org/10.1038/ncb1589

61. Thomson M, Liu SJ, Zou LN, Smith Z, Meissner A, Ramanathan S (2011) Pluripotency factors in embryonic stem cells regulate differentiation into germ layers. Cell 145(6): 875-889. https://doi.org/10.1016/j.cell.2011.05.017

62. Ahlfeld J, Favaro R, Pagella P, Kretzschmar HA, Nicolis S, Schüller U (2013) Sox2 requirement in sonic hedgehog-associated medulloblastoma. Cancer Res 73(12): 3796-3807. https://doi.org/10.1158/0008-5472.CAN-13-0238

63. Santini R, Pietrobono S, Pandolfi S, Montagnani V, D'Amico M, Penachioni JY, Vinci MC, Borgognoni L, Stecca B (2014) SOX2 regulates self-renewal and tumorigenicity of human melanoma-initiating cells. Oncogene 33(38): 4697-4708. https://doi.org/10.1038/onc.2014.71

64. Vanner RJ, Remke M, Gallo M, Selvadurai HJ, Coutinho F, Lee L, Kushida M, Head R, Morrissy S, Zhu X, Aviv T, Voisin V, Clarke ID, Li Y, Mungall AJ, Moore RA, Ma Y, Jones SJ, Marra MA, Malkin D, Northcott PA, Kool M, Pfister SM, Bader G, Hochedlinger K, Korshunov A, Taylor MD, Dirks PB (2014) Quiescent sox2(+) cells drive hierarchical growth and relapse in sonic hedgehog subgroup medulloblastoma. Cancer Cell 26(1): 33-47. https://doi.org/10.1016/j.ccr.2014.05.005

65. Tanaka S, Kamachi Y, Tanouchi A, Hamada H, Jing N, Kondoh H (2004) Interplay of SOX and POU factors in regulation of the Nestin gene in neural primordial cells. Mol Cell Biol 24(20): 8834-8846. https://doi.org/10.1128/MCB.24.20.8834-8846.2004

66. Kopp JL, Ormsbee BD, Desler M, Rizzino A (2008) Small increases in the level of Sox2 trigger the differentiation of mouse embryonic stem cells. Stem Cells 26(4): 903-911. https://doi.org/10.1634/stemcells.2007-0951

67 Wong YH, Lu AC, Wang YC, Cheng HC, Chang C, Chen PH, Yu JY, Fann MJ (2010) Protogenin defines a transition stage during embryonic neurogenesis and prevents precocious neuronal differentiation. J Neurosci 30(12): 4428-4439. doi: 10.1523/JNEUROSCI.0473-10.2010

68 Visvanathan A, Saulnier O, Chen C, Haldipur P, Orisme W, Delaidelli A, Shin S, Millman J, Bryant A, Abeysundara N, Wu X, Hendrikse LD, Patil V, Bashardanesh Z, Golser J, Livingston BG, Nakashima T, Funakoshi Y, Ong W, Rasnitsyn A, Aldinger KA, Richman CM, Van Ommeren R, Lee JJY, Ly M, Vladoiu MC, Kharas K, Balin P, Erickson AW, Fong V, Zhang J, Suárez RA, Wang H, Huang N, Pallota JG, Douglas T, Haapasalo J, Razavi F,

Silvestri E, Sirbu O, Worme S, Kameda-Smith MM, Wu X, Daniels C, MichaelRaj AK, Bhaduri A, Schramek D, Suzuki H, Garzia L, Ahmed N, Kleinman CL, Stein LD, Dirks P, Dunham C, Jabado N, Rich JN, Li W, Sorensen PH, Wechsler-Reya RJ, Weiss WA, Millen KJ, Ellison DW, Dimitrov DS, Taylor MD (2024) Early rhombic lip Protogenin+ve stem cells in a human-specific neurovascular niche initiate and maintain group 3 medulloblastoma. Cell S0092-8674(24)00651-2. doi: 10.1016/j.cell.2024.06.011

69. Roussel MF, Robinson GW (2013) Role of MYC in Medulloblastoma. Cold Spring Harb Perspect Med 3(11): a014308. https://doi.org/10.1101/cshperspect.a014308

70. Shih DJ, Northcott PA, Remke M, Korshunov A, Ramaswamy V, Kool M, Luu B, Yao Y, Wang X, Dubuc AM, Garzia L, Peacock J, Mack SC, Wu X, Rolider A, Morrissy AS, Cavalli FM, Jones DT, Zitterbart K, Faria CC, Schüller U, Kren L, Kumabe T, Tominaga T, Shin Ra Y, Garami M, Hauser P, Chan JA, Robinson S, Bognár L, Klekner A, Saad AG, Liau LM, Albrecht S, Fontebasso A, Cinalli G, De Antonellis P, Zollo M, Cooper MK, Thompson RC, Bailey S, Lindsey JC, Di Rocco C, Massimi L, Michiels EM, Scherer SW, Phillips JJ, Gupta N, Fan X, Muraszko KM, Vibhakar R, Eberhart CG, Fouladi M, Lach B, Jung S, Wechsler-Reya RJ, Fèvre-Montange M, Jouvet A, Jabado N, Pollack IF, Weiss WA, Lee JY, Cho BK, Kim SK, Wang KC, Leonard JR, Rubin JB, de Torres C, Lavarino C, Mora J, Cho YJ, Tabori U, Olson JM, Gajjar A, Packer RJ, Rutkowski S, Pomeroy SL, French PJ, Kloosterhof NK, Kros JM, Van Meir EG, Clifford SC, Bourdeaut F, Delattre O, Doz FF, Hawkins CE, Malkin D, Grajkowska WA, Perek-Polnik M, Bouffet

E, Rutka JT, Pfister SM, Taylor MD (2014) Cytogenetic prognostication within medulloblastoma subgroups. J Clin Oncol 32(9): 886-896. https://doi.org/10.1200/JCO.2013.50.9539

71. Sharma T, Schwalbe EC, Williamson D, Sill M, Hovestadt V, Mynarek M, Rutkowski S, Robinson GW, Gajjar A, Cavalli F, Ramaswamy V, Taylor MD, Lindsey JC, Hill RM, Jäger N, Korshunov A, Hicks D, Bailey S, Kool M, Chavez L, Northcott PA, Pfister SM, Clifford SC (2019) Second-generation molecular subgrouping of medulloblastoma: an international meta-analysis of Group 3 and Group 4 subtypes. Acta Neuropathol 138(2): 309-326. https://doi.org/10.1007/s00401-019-02020-0

72. Zeuner S, Vollmer J, Sigaud R, Oppermann S, Peterziel H, ElHarouni D, Oehme I, Witt O, Milde T, Ecker J (2024) Combination drug screen identifies synergistic drug interaction of BCL-XL and class I histone deacetylase inhibitors in MYC-amplified medulloblastoma cells. J Neurooncol 166(1): 99-112. https://doi.org/10.1007/s11060-023-04526-w

73. Liu J, Chi N, Zhang JY, Zhu W, Bian YS, Chen HG (2015) Isolation and characterization of cancer stem cells from medulloblastoma. Genet Mol Res 14(2): 3355-3361. https://doi.org/10.4238/2015

74. Li P, Lee EH, Du F, Gordon RE, Yuelling LW, Liu Y, Ng JM, Zhang H, Wu J, Korshunov A, Pfister SM, Curran T, Yang ZJ (2016) Nestin mediates hedgehog pathway tumorigenesis. Cancer Res 76(18): 5573-5583. https://doi.org/10.1158/0008-5472.CAN-16-1547

75. Gupta A, Kumar A, Abrari A, Patir R, Vaishya S (2016) Successful use of dose dense neoadjuvant chemotherapy and sodium valproate with minimal

toxicity in an infant with medulloblastoma in extremely poor general condition. World Neurosurg 93:485.e1-5. https://doi.org/10.1016/j.wneu.2016.07.044

76. Phiel CJ, Zhang F, Huang EY, Guenther MG, Lazar MA, Klein PS (2001) Histone deacetylase is a direct target of valproic acid, a potent anticonvulsant, mood stabilizer, and teratogen. J Biol Chem 276(39): 36734-36741. doi: 10.1074/jbc.M101287200

77. Gurvich N, Tsygankova OM, Meinkoth JL, Klein PS (2004) Histone deacetylase is a target of valproic acid-mediated cellular differentiation. Cancer Res 64(3): 1079-1086. doi: 10.1158/0008-5472.can-03-0799

Supplementary Information

Modulation of Stemness and Differentiation Regulators by Valproic Acid in Medulloblastoma

Natália Hogetop Freire • Alice Laschuk Herlinger • Júlia Vanini • Matheus Dalmolin • Marcelo A. C. Fernandes • Carolina Nör • Vijay Ramaswamy • Caroline Brunetto de Farias • André Tesainer Brunetto • Algemir L. Brunetto • Lauro José Gregianin • Mariane da Cunha Jaeger • Michael D. Taylor • Rafael Roesler

Supplementary Table 1. Forward and reverse primers used for RT-qPCR amplification.

Gene	Primer Forward (5'-3')	Primer Reverse (5'-3')
ACTB	AAACTGGAACGGTGAAGGTG	AGAGAAGTGGGGTGGCTTTT
CDKN1A	ACTCTCAGGGTCGAAAACGG	CTTCCTGTGGGCGGATTAGG
ENO2	AGCCTCTACGGGCATCTATGA	TTCTCAGTCCCATCCAACTCC
NES	GATCGCTCAGGTCCTGGAAG	GGGGTCCTAGGGAATTGCAG
MYC	TACAACACCCGAGCAAGGAC	AGCTAACGTTGAGGGGCATC
PTRG	TGCATGCAAGATTCATCCCACCC	TGCAATACTCCTGTTGGTAGGGCA
SOX2	CAGCTCGCAGACCTACATGA	GGGAGGAAGAGGTAACCACAG
TUBB3	CTCAGGGGCCTTTGGACATC	CAGGCAGTCGCAGTTTTCAC
TP53	ACCTATGGAAACTACTTCCTGAAA	CTGGGAGCTTCATCTGGACC

Supplementary Table 2. Primers targeting the promoter region of *TP53* in ChIP analysis.

Gene	Primer Forward (5'-3')	Primer Reverse (5'-3')
TP53	TTTAGCGCCAGTCTT GAGCA	GTATCTACGGCACCA GGTCG

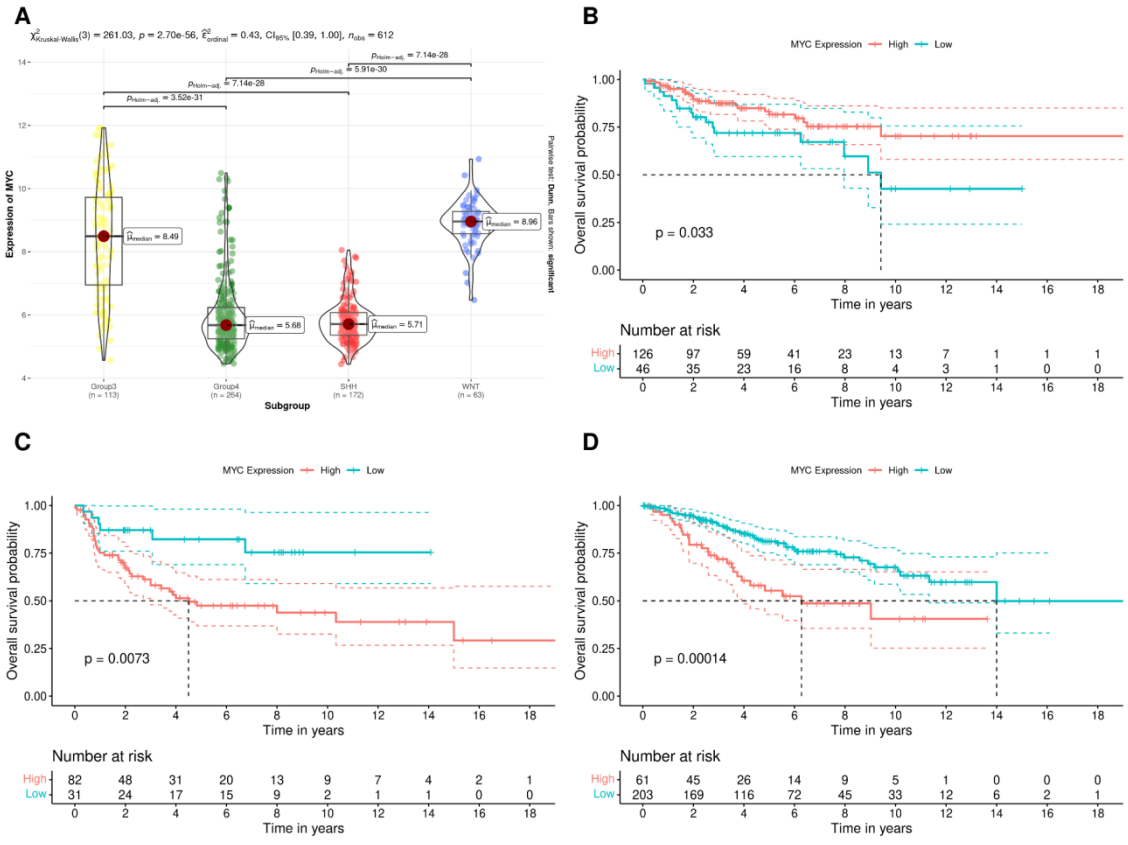

Supplementary Fig S1 *MYC* gene expression and association with patient prognosis across different molecular subgroups of human MB. **A** Transcript levels in group 3 (*n* = 113), group 4 (*n* = 264), SHH (*n* = 172), and WNT (*n* = 64). **B-D** OS of patients bearing MB tumors with high or low levels of *MYC* expression

classified into different molecular subgroups. Analyses were performed as described in Materials and Methods; *P* values are indicated in the figure.

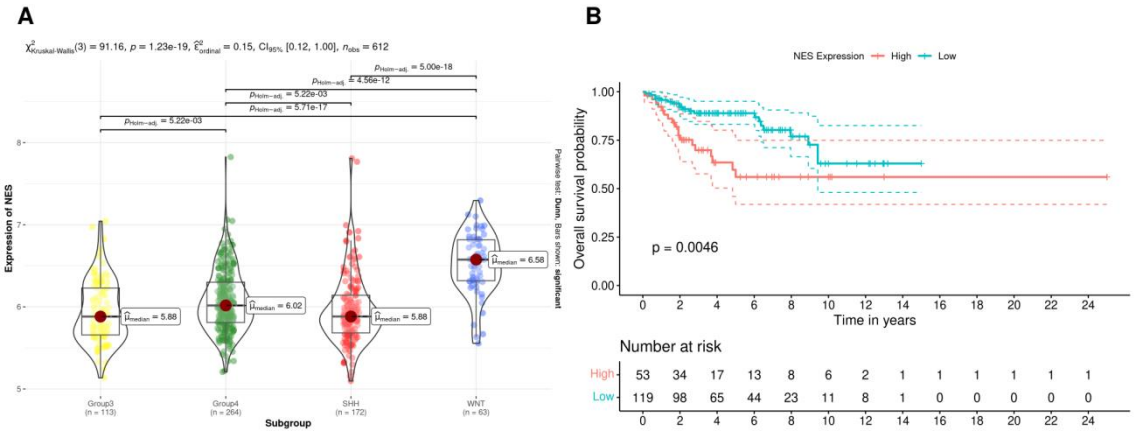

Supplementary Fig S2 *NES* gene expression across different molecular subgroups of human MB and association with prognosis in patients with SHH MB. **A** Transcript levels in group 3 (*n* = 113), group 4 (*n* = 264), SHH (*n* = 172), and WNT (*n* = 64). **B** OS of patients bearing SHH MB tumors with high or low levels of *NES* expression. Analyses were performed as described in Materials and Methods; *P* values are indicated in the figure.

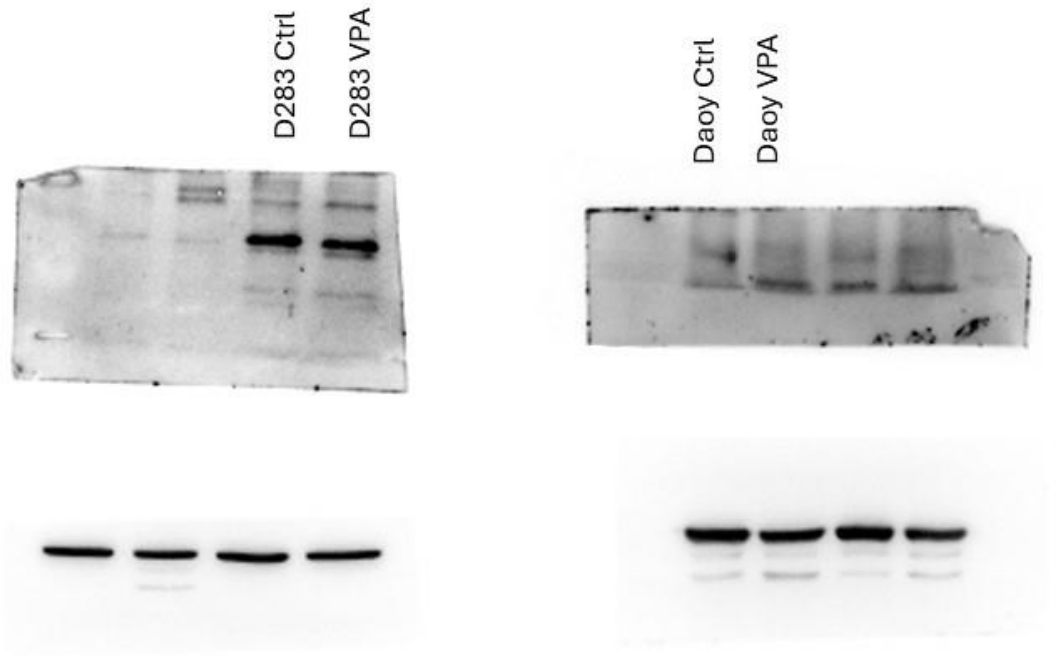

Supplementary Fig S3 Uncropped blots for the experiment shown in Fig. 2C describing the Western blot analysis of p21 protein in D283 and Daoy MB cells.